DOI: 10.13009/EUCASS2022-7135
9TH EUROPEAN CONFERENCE FOR AERONAUTICS AND SPACE SCIENCES (EUCASS)

Wind Estimation for Small Fixed-Wing UAV Using Standard Sensors

Béatrice Jacquier, Thierry Le Moing and Guido Magnani
ONERA / DTIS, Université de Toulouse
F-31055 Toulouse, France

Abstract

An approach of wind estimation using Fixed-Wing Unmanned Aerial Vehicles is proposed based on measurements provided by a standard sensor suite and simplified aerodynamic models used as virtual sideslip and incidence sensors. In a first step, virtual sensors models parameters and Pitot tube calibration factor are estimated by off-line estimation methods as Iterated Extended Kalman Smoother, Filter-error minimization and Maximum a posteriori. Specific manoeuvres and quiet atmosphere are required. In a second step, on-line wind estimation is realised by an EKF based on calibrated models and able to estimate a sudden wind gust with no delay as well as turbulence.

1. Introduction

Small Fixed-Wing Unmanned Aerial Vehicles (FWUAVs) are very sensitive to wind since its magnitude is comparable to the FWUAV speed. Moreover, their small size and the limitation of their propulsion system and actuation capability make it difficult to maintain control in windy conditions. In order to limit wind impact in FWUAV attitude and trajectory, instantaneous wind velocity estimation can be introduced in control laws.
When the velocity of the aircraft relative to the airmass is available, wind speed vector may be computed directly or estimated using geometric relations between velocity of the aircraft relative to ground, velocity of the aircraft relative to the airmass and wind speed vectors, called the "wind triangle" equations (cf. paragraph 2.1). However, this necessitates the aircraft to be equipped with sensors able to measure the three components of the airspeed vector typically either with a multi-hole Pitot probe [11, 15], or a simple Pitot probe and vanes to measure angle of attack (AOA) and angle of sideslip (SSA) [3, 5, 2]. However, unlike larger aircrafts, small FWUAVs do not usually have sensors dedicated to measurement of these variables due to difficulties encountered in their installation, to their cost and to aerodynamic flow disturbances nearby fuselage.
Another approach, frequently used to estimate SSA on board transport aircrafts, consists in replacing SSA measurement by its estimate obtained from aerodynamic modelling, Pitot tube and IMU (Inertial Measurement Unit) measurements. This approach is referred to as a virtual sensor. In [12] airspeed, AOA and SSA are estimated from GNSS (Global Navigation Satellite System), IMU and a model of the aircraft's dynamics. But this approach is based on a reliable aerodynamic model, which may be tuned from wind tunnel or flight tests. Such models are seldom available for small UAV applications.
We are then interested, in this paper, in the challenge of onboard FWUAV wind speed estimation without having at one's disposal neither SSA and AOA measurements nor a reliable aerodynamics model. In [4], a horizontal wind speed vector is estimated by an EKF (Extended Kalman Filter) which uses only measurements provided by GPS, IMU and a simple Pitot tube. Calibration of the Pitot tube sensor is realised simultaneously. The estimator model is based only on the wind triangle equations. The proposed estimation method necessitates headings variations during the flight in order to make the states observable. In [8] this approach is generalised to a three-dimensional wind. Contrary to the estimator model used in [4], the model is linear with respect to the state then a simple Kalman Filter is used. Model linearity is used to demonstrate that state observability is obtained through attitude variations during the flight. The work presented in [1] aims at improving estimators of [4] and [8] including "pseudo-measurements" of SSA and AOA. The objective is to be able to estimate wind even without attitude variations. The proposed "pseudo-measurements" consist in constant equilibrium values of SSA and AOA which implies that AOA and SSA variations around their equilibrium values have to be small. In [17] the approach of [8] is extended by adding a vertical acceleration measurement. In this work, the wind is modelled as a sum of steady, slowly changing wind and turbulent wind. The turbulent wind model is the Dryden model. Assuming that steady and turbulent wind act at different frequencies, they are estimated separately introducing a frequency separation on parameters. Turbulent wind states are then estimated from the vertical

DOI: 10.13009/EUCASS2022-7135

acceleration measurement together with a simplified vertical aerodynamic model whose coefficients are estimated simultaneously with the wind states.
A survey on wind estimation using FWUAV is proposed in [16].
Based on those previous works, we propose an approach for wind estimation using small FWUAV which is based on measurements provided by a standard sensor suite (GPS, IMU and a simple Pitot tube) and simplified aerodynamic models used as virtual AOA and SSA sensors. Virtual sensors models are based on relationships between data coming from Pitot tube, accelerations and actuators deflections, and some aerodynamic parameters which need to be estimated. It is also necessary to estimate a scaling factor for Pitot tube measurement calibration. As it was demonstrated in previous works, attitude changes are necessary for a concurrent estimation of wind speed, aerodynamic parameters and Pitot tube scaling factor. As we expect to estimate wind velocity in all flight phases including straight flight, with a large bandwidth, our approach is divided in two steps. In the first one virtual sensors parameters and Pitot tube calibration factor are estimated from specific exciting manoeuvres, whereas in the second step Pitot tube and virtual sensors calibrated in the first step are used to perform on-line wind estimation for all flight phases. For this latter, estimation is carried out by an EKF. Calibration estimators however don't need to operate on-line. Then different estimation algorithms have been tested: EKF, Iterated Extended Kalman Smoother (IEKS), Filter-error minimization (FE), Output-error minimization (OE) and Maximum a posteriori (MAP).
The remainder of this paper is organized as follows. Section 2 provides a detailed description of the different models used in this work. In Section 3 the different estimation / identification methods are described. Then, Section 4 presents the simulated results in a Matlab/Simulink environment of the different steps of the estimation process. The calibration step is presented Sec. 4.1 and the on-line wind estimation in Sec. 4.2.

2. Models

2.1 Kinematic model

Let $V_{k0} = [u_{k0}\ v_{k0}\ w_{k0}]^T$ refer to the velocity of the aircraft relative to earth, $V_0 = [u_0\ v_0\ w_0]^T$ the velocity of the aircraft relative to the wind and $V_{w0} = [u_{w0}\ v_{w0}\ w_{w0}]^T$ the velocity of the wind relative to earth, all expressed in a Earth fixed North-East-Down coordinate frame. The relation ship between these velocities, also called the "wind triangle", expressed in the Earth frame is:

$$\begin{cases} u_0 &= u_{k0} - u_{w0} \\ v_0 &= v_{k0} - v_{w0} \\ w_0 &= w_{k0} - w_{w0} \end{cases} \tag{1}$$

The rotation matrix from the Earth frame to a body-fixed coordinate frame is denoted as $\mathrm{R}_{e\to b}$ and is defined by the roll (ϕ), pitch (θ) and yaw (ψ) angles. Hence, the velocity of the aircraft relative to the wind, expressed in the body frame as $V = [u\ v\ w]^T$, is:

$$\begin{bmatrix} u \\ v \\ w \end{bmatrix} = \mathrm{R}_{e\to b}(\phi, \theta, \psi) \begin{bmatrix} u_0 \\ v_0 \\ w_0 \end{bmatrix} \tag{2}$$

The sideslip angle (β) and the angle of attack (α) are the angles between the body-fixed axes of the aircraft and its velocity vector relative to the wind V:

$$\beta = \arcsin\left(v/V_a\right) \tag{3}$$

$$\alpha = \arctan\left(w/V_a\right) \tag{4}$$

with $V_a = (u^2 + v^2 + w^2)^{1/2} = (u_0^2 + v_0^2 + w_0^2)^{1/2}$ the modulus of the air speed.

2.2 Wind model

We assume the wind is slowly time-varying relative to Earth then evolution model chosen for wind components is:

$$\begin{cases} \dot{u}_{w0}(t) &= \xi_1(t) \\ \dot{v}_{w0}(t) &= \xi_2(t) \\ \dot{w}_{w0}(t) &= \xi_3(t) \end{cases} \tag{5}$$

with $\xi_1(t)$, $\xi_2(t)$ and $\xi_3(t)$ zero mean Gaussian white noises.

DOI: 10.13009/EUCASS2022-7135

2.3 Measurement models

We assume that the components of the velocity of the aircraft relative to earth in Earth frame $V_{k0} = [u_{k0}\ v_{k0}\ w_{k0}]^T$ are measured with sufficient accuracy by an onboard GNSS. We assume as well that an onboard IMU / Attitude and Heading Reference System (AHRS) delivers accurate measurements of accelerations (r_x, r_y and r_z) and angular rates (p, q and r) of the aircraft in the body frame, and attitude angles (ϕ, θ and ψ). Finally, control surfaces deflection measurements are also supposed available and non noisy.

Airspeed measurement model

A Pitot static tube is used to provide a measurement of the airspeed (V_a). It delivers a measurement of the difference between the total pressure at the tip of the probe (P_T) and the static pressure at the side of the probe (P_S). Assuming this difference is small, the relationship between airspeed and pressure difference may be approximated by Bernouilli's equation as follows:

$$V_a = (2\Delta P/\rho)^{1/2} \tag{6}$$

with $\Delta P = P_T - P_S$ and ρ the air density.
For a perfect gas, the air density is expressed as $\rho = P_S/(RT_S)$ with T_S the static temperature and $R = 287$ J.kg^{-1}.K^{-1} the air individual gas constant. The static temperature comes from a temperature probe which provides a low accuracy measurement of total temperature. The airspeed measurement model chosen is then:

$$V_m = (2\Delta P/\rho)^{1/2} = k\ \left(u_0^2 + v_0^2 + w_0^2\right)^{1/2} + \nu_1 \tag{7}$$

with k, a calibration factor, and ν_1, a Gaussian white measurement noise, that both compensate for model assumptions, probe installation errors and sensors errors and noises.

Virtual sensors models

From the kinematic model equations presented in section 2.1 we see that components of the velocity of the wind relative to earth may be directly computed from the aforementioned measurements if AOA and SSA measurements are also available. As we assume no such sensors are available onboard, we will use acceleration measurements (provided by IMU) and a simplified aerodynamic models in order to estimate those angles. This approach is referred to as a virtual sensors.
Lateral and vertical accelerations of the aircraft in the body frame may be modelled this way:

$$\begin{aligned} r_y &= -\rho\ V_a^2\ S\ C_Y\ /\ (2\ m) \\ r_z &= \rho\ V_a^2\ S\ (\cos\alpha\ C_L + \sin\alpha\ C_D)\ /\ (2\ m) \end{aligned} \tag{8}$$

with C_D, C_Y and C_L respectively the drag, lateral and lift aerodynamic coefficients, S the reference surface and m the mass of the aircraft. Those coefficients may be modelled by:

$$\begin{aligned} C_D &= C_{D_0} + C_{D_\alpha}\ \alpha + C_{D_{\alpha 2}}\ \alpha^2 \\ C_Y &= C_{Y_\beta}\ \beta + (L_{lat}/V_a)\ (C_{Y_p}\ p + C_{Y_r}\ r) + C_{Y_{\delta_r}}\ \delta_r + C_{Y_{\delta_a}}\ \delta_a \\ C_L &= C_{L_0} + C_{L_\alpha}\ \alpha + (L_{lon}/V_a)\ C_{L_q}\ q + C_{L_{\delta_e}}\ \delta_e \end{aligned} \tag{9}$$

with L_{lat} and L_{lon} the lateral and the longitudinal reference length respectively and δ_a, δ_e, δ_r the ailerons, elevators and rudder deflection respectively. Assuming angles α and β are small and δ_e, δ_a, p and r effects are negligible then eq. (8) simplifies to:

$$\begin{aligned} r_y &\approx -\rho\ V_a^2\ S\ (C_{Y_\beta}\ \beta + C_{Y_{\delta_r}}\ \delta_r)\ /\ (2\ m) \\ r_z &\approx \rho\ V_a^2\ S\ \left(C_{L_0} + (C_{D_0} + C_{L_\alpha})\ \alpha + (L_{lon}/V_a)\ C_{L_q}\ q\right)\ /\ (2\ m) \end{aligned} \tag{10}$$

Virtual SSA and AOA models chosen are then:

$$\begin{aligned} r_{y_m} &= \rho_0\ r_y/\rho = -\rho_0\ V_a^2\ S\ (\tilde{C}_{Y_\beta}\ \beta + \tilde{C}_{Y_{\delta_r}}\ \delta_r)\ /\ (2\ m) + \nu_2 \\ r_{z_m} &= \rho_0\ r_z/\rho = \rho_0\ V_a^2\ S\ \left(\tilde{C}_{L_0} + \tilde{C}_{L_\alpha}\ \alpha + (L_{lon}/V_a)\ \tilde{C}_{L_q}\ q\right)\ /\ (2\ m) + \nu_3 \end{aligned} \tag{11}$$

with $\rho_0 = 1.225$ kg/m^2 the air density at sea level and ν_2 and ν_3 Gaussian white measurement noise that take into account sensor noise and model error.

Without knowledge of the UAV aerodynamic model, methods from statistical field theory can be used to determine an adequate model structure. The well-established modified stepwise regression method was implemented to determine the structure of the virtual sensor models. This method initially proposed in [7] was successfully used by Klein [9] in the field of aerodynamic model identification to determine aircraft model structure from flight data.

DOI: 10.13009/EUCASS2022-7135

This iterative technique serves to decide which regressors to include, to evaluate if the regressor decreased significantly a cost criteria, and to determine when to stop including regressors. The first step is the forward selection step. It is used to choose the new regressor among the remaining regressors which provides the greatest reduction of the cost criteria. Adding a new regressor may make previously added regressors irrelevant, a backward elimination step has to be performed. During this step, regressors that no longer decrease the cost criteria are removed. This procedure is repeated until there is no longer significant reduction of the cost criteria.
In the present study, virtual sensor models are assumed to consist of a bias and linear terms with respect to flight parameters and control surface deflections. As all these variables are not directly measured, the stepwise regression procedure was implemented with an output-error method to estimate parameter values of the sensor models. Figure 1 illustrates the results of this technique obtained with simulated data presented in paragraph 4.1. The upper plot presents the evolution of the selected variables during the iterations, whereas the lower plot shows the decrease of a quadratic error criteria. Structure of the selected model is finally identical to that one resulting from the approximation of the aerodynamic models.

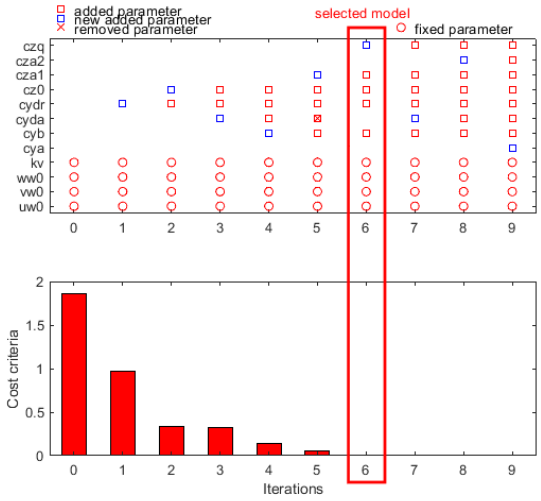

Figure 1: Stepwise regression procedure for sensor models structure determination

3. Estimation methods

In this section, we detail different estimation/identification methods tested. First of all, as the final goal is to estimate, on-line, the components of the wind velocity vector relative to earth, we use an Extended Kalman Filter (EKF) method in the second step of the procedure.
For the first step (calibration step), it is also possible to perform calibration using an EKF but, as the processing may be realised off-line, other methods may be used that (as we will see) give better results in comparison with the EKF approach.
Consider a nonlinear continuous state space representation of a dynamic system with discrete-time observations:

$$\begin{aligned} \dot{x}(t) &= f\left(x(t), \theta, u(t)\right) + \xi(t) \\ y(t) &= h\left(x(t), \theta, u(t)\right) \\ z_k &= y(t_k) + v(t_k) \quad \text{for } t_k = k\Delta t \text{ and } k = 0, \ldots, N \\ x(0) &= x_0 \end{aligned} \tag{12}$$

t refers to the continuous time variable, whereas k defines the discrete time index relative to a sampling period (Δt). f and h are assumed to be known vector functions depending on the state vector $x(t)$, on the input vector $u(t)$ vectors and on a parameters vector which has to be identified (θ). y is the model output vector. ξ is a zero mean Gaussian white noise with power spectral density (Q), v is a zero mean Gaussian pseudo-white noise with covariance (R), and x_0 is a random vector with mean ($\overline{x_0}$) and covariance (P_0) modelling the initial state vector.

Extended Kalman Filter, Extended Kalman Smoother, Iterated Extended Kalman Smoother

The Extended Kalman Filter is a state estimator which operates in two steps: a prediction step and a filtering step.

DOI: 10.13009/EUCASS2022-7135

The prediction step computes an estimation of the state vector at time t_k, $\hat{x}(t_k|t_{k-1})$, and its covariance matrix, $P(t_k|t_{k-1})$, given the past measurements z_i for $i = 0 : k-1$, the state estimate at t_{k-1}, $\hat{x}(t_{k-1}|t_{k-1})$, and the associated state error covariance matrix $P(t_{k-1}|t_{k-1})$:

$$\hat{x}(t_k|t_{k-1}) = \hat{x}(t_{k-1}|t_{k-1}) + \int_{t_k}^{t_{k+1}} f\left(x(t), \theta, u(t)\right) dt \tag{13}$$

$$P(t_k|t_{k-1}) = \Phi(t_{k-1})\, P(t_{k-1}|t_{k-1})\, \Phi^T(t_{k-1}) + \Delta t\, Q \tag{14}$$

with $\Phi(t_{k-1}) = \exp\left(A(t_{k-1})\Delta t\right)$ the transition matrix and $A(t_{k-1})$ referring to the linearised state equation with regards to $x(t)$ at t_{k-1} such:

$$A(t_{k-1}) = \left.\frac{\partial f(x(t), \theta, u(t))}{\partial x(t)}\right|_{x(t)=\hat{x}(t_{k-1}|t_{k-1})} \tag{15}$$

The filtering step consists in updating the state vector taking into account the information given by a new available measurement. Thus, when a new measurement vector z_k is available at time t_k, the predicted state vector $\hat{x}(t_k|t_{k-1})$ is corrected in order to produce the estimate $\hat{x}(t_k|t_k)$ and its associated state error covariance matrix $P(t_k|t_k)$:

$$\hat{x}(t_k|t_k) = \hat{x}(t_k|t_{k-1}) + K(t_k)\ \left(z(t_k) - h\left(\hat{x}(t_k|t_{k-1}), \theta, u(t_{k-1})\right)\right) \tag{16}$$

$$P(t_k|t_k) = P(t_k|t_{k-1}) - K(t_k)\, C(t_k)\, P(t_k|t_{k-1}) \tag{17}$$

with $K(t_k)$ the Kalman matrix gain expressed as $K(t_k) = P(t_k|t_{k-1})\, C^T(t_k)\, S(t_k)^{-1}$, $S(t_k)$ the covariance matrix of the output prediction error expressed as $S(t_k) = C(t_k)\, P(t_k|t_{k-1})\, C^T(t_k) + R$, and $C(t_k)$ referring to the linearised observation equation with regards to $x(t)$:

$$C(t_k) = \left.\frac{\partial h(x(t), \theta, u(t))}{\partial x(t)}\right|_{x(t)=\hat{x}(t_k|t_{k-1})} \tag{18}$$

The EKF computes at each time step t_k an on-line estimation of the state given the measurements up to t_k and the past states estimates. The state estimate may be improved, off-line, taking into account the overall measurements as well as the successive states and covariances estimated within a process called smoothing. With the Rauch smoother [14], a new state estimate $\hat{x}(t_k|t_{0:N})$ and its covariance matrix $P(t_k|t_{0:N})$ are derived in a backward recursion such:

$$\begin{aligned} \hat{x}(t_k|t_{0:N}) &= \hat{x}(t_k|t_k) - K_s(t_k)\ \left(\hat{x}(t_{k+1}|t_k) - \hat{x}(t_{k+1}|t_{0:N})\right) \\ P(t_k|t_{0:N}) &= P(t_k|t_k) - K_s(t_k)\ \left(P(t_{k+1}|t_k) - P(t_{k+1}|t_{0:N})\right)\ K_s(t_k)^T \end{aligned} \tag{19}$$

with $K_s(t_k) = P(t_k|t_k)\, \Phi(t_k)\, P(t_{k+1}|t_k)^{-1}$.
The process is initialised by $\hat{x}(t_N|t_{0:N}) = \hat{x}(t_N|t_{N-1})$ and $P(t_N|t_{0:N}) = P(t_N|t_{N-1})$.
At the end of the smoothing process a new estimate of the state at time t_0 is provided, then this new value can be used to initialise a new filtering/smoothing step. This is the principle of the Iterative Extended Kalman Smoother (IEKS) method where these operations are repeated iteratively until convergence.

Maximum likelihood estimators

In the previously described estimators, the parameter vector θ was supposed to be known. With the filter error method (FE) [13, 10], both parameters and states are estimated. The principle of the method is to find the parameter vector θ that maximises the likelihood function, that means the probability of measured outputs given a set of parameters. Evolution noise is taken into account by means of an EKF for state estimate. The maximum likelihood estimate is:

$$\begin{aligned} \underset{\theta}{\operatorname{argmax}}\ \left(L(\theta)\right) = \underset{\theta}{\operatorname{argmax}}\ \left(p(z_{0:N}|\theta)\right) &= \underset{\theta}{\operatorname{argmin}}\ \left(-\ln p(z_{0:N}|\theta)\right) \\ &= \underset{\theta}{\operatorname{argmin}} \left(\sum_{k=0}^{N} \left[z_k - \hat{y}_\theta(t_k)\right]^T S_k^{-1} \left[z_k - \hat{y}_\theta(t_k)\right] \right) \end{aligned} \tag{20}$$

with z_k vector of measured outputs at instant t_k, $\hat{y}_\theta(t_k) = h(\hat{x}(t_k|t_{k-1}), \theta, u(t_{k-1}))$ vector of the predicted outputs at instant t_k given by an EKF, for the value θ of parameters, and S_k covariance matrix of the output prediction error $(z_k - y_\theta(t_k))$.
Minimisation is realised iteratively. At each iteration, predicted outputs vector and output prediction error covariance matrix for each instant are estimated from the current value of the parameters. Then a new parameter vector is determined, minimising the cost function of eq. (20). This minimisation is realised by a Gauss-Newton type algorithm.

DOI: 10.13009/EUCASS2022-7135

Iterations are repeated until convergence to parameter vector $\hat{\theta}$.
Thanks to the Cramer Rao inequality, an approximation of the estimated parameters covariance matrix is given by:

$$\mathrm{Cov}\{\hat{\theta}\} \approx \left(\sum_{k=0}^{N} \left(\left. \frac{\partial \hat{y}_\theta(t_k)}{\partial \theta} \right|_{\theta=\hat{\theta}}^{T} S_k^{-1} \left. \frac{\partial \hat{y}_\theta(t_k)}{\partial \theta} \right|_{\theta=\hat{\theta}} \right) \right)^{-1} \tag{21}$$

From this covariance matrix we can derive the Cramer Rao bound for parameter i expressed as [13] $\sigma_i = \left(\left[\mathrm{Cov}\{\theta\}^{-1} \right]_{ii} \right)^{1/2}$ which is a measure of accuracy of the estimated parameters.

The output-error method (OE) corresponds to the filter error method with the process noise neglected and a stable evolution model. The states are then computed deterministically by direct numerical integration. The maximum likelihood estimator becomes:

$$\underset{\theta}{\mathrm{argmax}} \ (L(\theta)) = \underset{\theta}{\mathrm{argmin}} \left(\sum_{k=0}^{N} \left[z_k - h(\hat{x}(t_k), \theta, u(t_k)) \right]^T R^{-1} \left[z_k - h(\hat{x}(t_k), \theta, u(t_k)) \right] \right) \tag{22}$$

with

$$\hat{x}(t_k) = \hat{x}(t_{k-1}) + \int_{t_k}^{t_{k+1}} f(x(t), \theta, u(t)) dt \tag{23}$$

Maximum a posteriori estimator (MAP)

The principle of the maximum a posteriori estimator is to find the set of parameters θ and the time dependent sequence of states $x_{0:N} = [x(t_0), \ldots, x(t_N)]^T$ which maximises the posterior probability, that means the probability of the parameters and the states given the measurements. Following Bayes' rule the posterior probability is:

$$p(x_{0:N}, \theta \mid z_{0:N}) = \frac{p(z_{0:N} \mid x_{0:N}, \theta)\ p(x_{0:N})}{p(z_{0:N})} \propto p(x_0, \theta) \prod_{k=0}^{N} p(z_k \mid x_k, \theta) \prod_{k=0}^{N-1} p(x_{k+1} \mid x_k, \theta) \tag{24}$$

Assuming that the density $p(x_0, \theta)$ is a uniform distribution (no prior information on x_0 and θ), then the MAP estimator expresses as [6]:

$$\begin{aligned} \underset{x_{0:N},\theta}{\mathrm{argmax}} \ (p\,(x_{0:N}, \theta \mid z_{0:N})) &= \underset{x_{0:N},\theta}{\mathrm{argmin}} \ (-\ln p\,(x_{0:N}, \theta \mid z_{0:N})) \\ &= \underset{x_{0:N},\theta}{\mathrm{argmin}} \left(\sum_{k=0}^{N} \left(\left[z_k - h\,(x_k, \theta, u(t_k)) \right]^T R^{-1} \left[z_k - h\,(x_k, \theta, u(t_k)) \right] \right) \right. \\ &\left. + \sum_{k=0}^{N-1} \left(\left[x_{k+1} - x_k - \int_{t_k}^{t_{k+1}} f\,(x(t), \theta, u(t))\, dt \right]^T (\Delta t\ Q)^{-1} \left[x_{k+1} - x_k - \int_{t_k}^{t_{k+1}} f\,(x(t), \theta, u(t))\, dt \right] \right) \right) \end{aligned} \tag{25}$$

The estimate can be obtained by solving a nonlinear constrained optimization problem. We will see that in our case it simplifies to a non-constrained problem that can be solved by a Gauss Newton type algorithm. An approximation of the estimated parameters covariance matrix is given by:

$$\mathrm{Cov}\{\hat{\Theta}\} = \left(\sum_{k=0}^{N} \left(\left. \frac{\partial h(x_k, \theta, u(t_k))}{\partial \Theta} \right|_{\Theta=\hat{\Theta}}^{T} R^{-1} \left. \frac{\partial h(x_k, \theta, u(t_k))}{\partial \Theta} \right|_{\Theta=\hat{\Theta}} \right) + \sum_{k=0}^{N-1} \left(\left. \frac{\partial \epsilon_k}{\partial \Theta} \right|_{\Theta=\hat{\Theta}}^{T} (\Delta t\ Q)^{-1} \left. \frac{\partial \epsilon_k}{\partial \Theta} \right|_{\Theta=\hat{\Theta}} \right) \right)^{-1} \tag{26}$$

with $\Theta = [x_{0:N},\ \theta]^T$, $\hat{\Theta}$ the estimated vector and $\epsilon_k = x_{k+1} - x_k - \int_{t_k}^{t_{k+1}} f(x(t), \theta, u(t)) dt$

4. Simulation results

Simulations are performed from a generic nonlinear model representative of the fight dynamics of a 50 kg fixed wings UAV, flying at approximately 25 m/s. The objective scenario is straight and level flight then control/guidance laws are added in order to maintain a straight trajectory at constant altitude.
Reference values for parameters of the virtual sensor models described in eq. (11), derived from the nonlinear model, are $k = 1$, $\tilde{C}_{Y_\beta} = -0.32$, $\tilde{C}_{Y_{\delta_r}} = 0.21$, $\tilde{C}_{L_0} = 0.46$, $\tilde{C}_{L_\alpha} = 4.97$ and $\tilde{C}_{L_q} = 8.15$. Simulated airspeed measurement Vm, computed from eq. (7), is perturbed by a Gaussian noise of standard deviation 1 m/s whereas lateral and vertical

DOI: 10.13009/EUCASS2022-7135

simulated accelerations of the aircraft in the body frame are both perturbed by a Gaussian noise of standard deviation 0.2 m/s^2. Simulated data are provided at a rate of 100 Hz and down sampled to a rate of 25 Hz.
Within this simulation environment, the response of the UAV to a mean wind as well as to a turbulence wind disturbance is also considered. Turbulence wind is generated by passing white noise through a low pass filter. The filter is designed according to the Dryden model.

4.1 Virtual sensors and Pitot tube calibration

As measurements equations 11 are decoupled, SSA and AOA virtual sensors calibration will be carried out separately.

Virtual sideslip angle sensor and Pitot tube calibration

The general model used for estimation is the one presented in eq. (12). The evolution model for the components of the wind velocity is the model of eq. (5) then we have $f(x(t), \theta, u(t)) = 0$ in (12). Measurements used for estimation are the modulus of the airspeed (V_m) and the lateral acceleration (r_{y_m}) with estimator observation equations respectively given in eq. (7) and eq. (11). The covariance matrix of the measurement noise is $R = \text{diag}([r_1^2,\ r_2^2])$ with $r_1 = 1$ m/s and $r_2 = 0.2$ m/s^2.

In a first instance, a particular manoeuvre is defined in order to estimate accurately virtual SSA sensor calibration parameters ($\tilde{C}_{Y_\beta}$ and $\tilde{C}_{Y_{\delta_r}}$) and Pitot tube calibration factor (k). As shown in [8] manoeuvres with attitude variations are necessary for the wind components to be observable from the measurement of the airspeed. Moreover, SSA changes are required for $\tilde{C}_{Y_\beta}$ and $\tilde{C}_{Y_{\delta_r}}$ to be observable from the lateral acceleration measurement.
The chosen manoeuvre, presented in Figure 2, is composed of a 30 degrees roll angle constant turn with lateral acceleration oscillations of period 20 s. These oscillations result from a train of doublets as commanded signal on lateral acceleration. A constant mean horizontal wind is also simulated with components $u_{w0} = 5\ m/s$, $u_{w0} = 6\ m/s$ and $u_{w0} = 0\ m/s$.

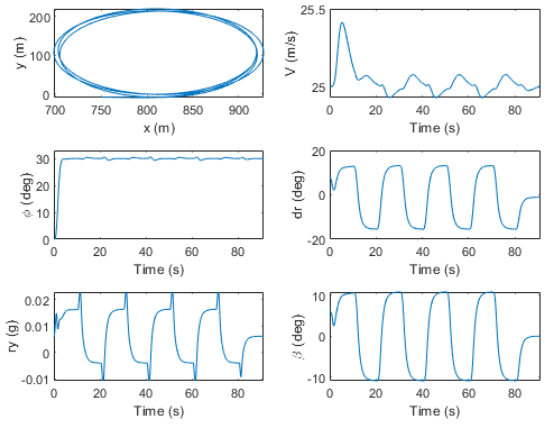

Figure 2: Lateral calibration manoeuvre

First, components of the mean wind velocity and calibration parameters are estimated using output error minimisation method from a non noisy simulation. Applying this method requires the evolution noise to be null ($\xi(t) = 0$ in eq. (12) then only the observation equation is considered. Estimator of eq. (22) is applied with $\theta = [u_{w0},\ u_{w0},\ u_{w0},\ k,\ \tilde{C}_{Y_\beta},\ \tilde{C}_{Y_{\delta_r}}]^T$. This estimator, not suitable for non constant wind, gives informations on the observability of the parameters. The Cramer Rao bounds on the estimated parameters given by the method are σ_θ =[0.024, 0.024, 0.11, 0.0008, 0.049, 0.037]. It indicates that uncertainty on the vertical component of the wind is important. The correlation matrix of estimated parameters is presented in Figure 3. It reveals that parameter w_{w0} is strongly correlated with $\tilde{C}_{Y_\beta}$ and $\tilde{C}_{Y_{\delta_r}}$. Imposing a constraint on w_{w0} allows to remove this correlation and improve the observability of $\tilde{C}_{Y_\beta}$ and $\tilde{C}_{Y_{\delta_r}}$. In the following of this section, we then impose $w_{w0} = 0$ in the estimators models. For the MAP estimator, where we can easily impose the mean value of w_{w0} estimate be zeros, we test also this constraint. With the constraint $w_{w0} = 0$ in the output error model, estimated parameters standard deviation becomes σ_θ =[0.024, 0.024, 0.0008, 0.018, 0.014]. Uncertainty on SSA virtual sensor calibration parameters has been decreased. Correlation matrix reveals also a correlation between $\tilde{C}_{Y_\beta}$ and $\tilde{C}_{Y_{\delta_r}}$ which comes from the control signal. Because of this correlation, the initial parameters values used in the estimation process have to be rather accurate, and particularly the initial value of parameter k.

DOI: 10.13009/EUCASS2022-7135

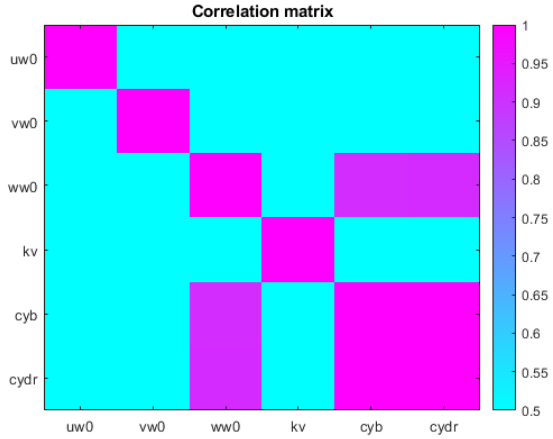

Figure 3: Correlation matrix on estimated parameters (OE lateral calibration manoeuvre)

Lateral calibration parameters are now estimated with an EKF. The estimator model is described in eq. (12) with $x = [u_{w0},\ v_{w0},\ k,\ \tilde{C}_{Y_\beta},\ \tilde{C}_{Y_{\delta_r}}]^T$, $Q = \text{diag}([q_1^2,\ q_2^2,\ 0,\ 0,\ 0])$ and $P_0 = \text{diag}([p0_1,\ p0_2,\ p0_3,\ p0_4,\ p0_5])$. Figure 4 presents the evolution of estimated state function of time for a simulation including measurement noise and with $q_1 = q_2 = 0.1$ m/s$^{\frac{3}{2}}$. From this Figure we observe that $\tilde{C}_{Y_\beta}$ and $\tilde{C}_{Y_{\delta_r}}$ converge slowly to their real value. This is due to the correlation between those two parameters which makes them weakly observable. Tuning chosen for the evolution noise corresponds to the maximum possible evolution noise, increasing this one leads to divergence of the estimator. Turbulence wind model is not taken into account in our estimator model then it is considered as a perturbation noise acting on the state derivative. We can then derive a turbulence wind level corresponding to the evolution noise level: $\sigma_x = \sigma_y = 0.2$ m/s and $\sigma_z = 0.15$ m/s. This level is under the level of a weak turbulence ($\sigma_x = \sigma_y = 0.96$ m/s and $\sigma_z = 0.7$ m/s) then calibration flights have to be performed in quite atmosphere. Afterwards, this turbulence level is retained for simulation of calibration flights.

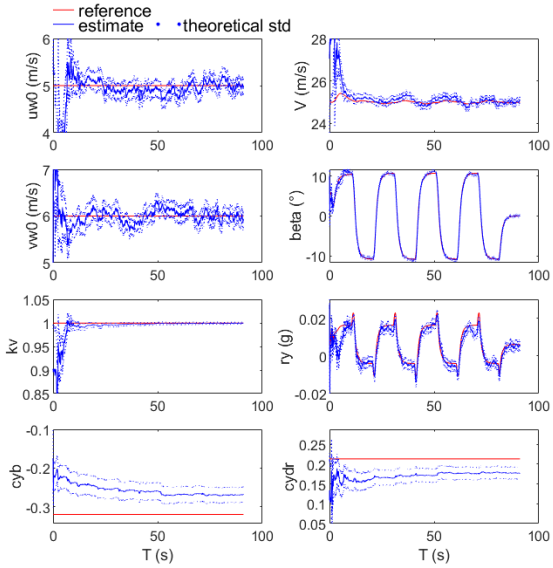

Figure 4: EKF lateral calibration model with output noise

As the calibration process does not need to be performed on-line, results of the EKF may be improved using off-line estimation methods. IEKS, EF and MAP methods have been tested. IEKS algorithm is applied to the aforementioned model used for EKF whereas the filter error estimator of eq. (20) and the maximum a posteriori estimator of eq. (25) are applied with the estimator model of eq. (12) such that $x = [u_{w0},\ v_{w0}]^T$ and $\theta = [k,\ \tilde{C}_{Y_\beta},\ \tilde{C}_{Y_{\delta_r}}]^T$.

DOI: 10.13009/EUCASS2022-7135

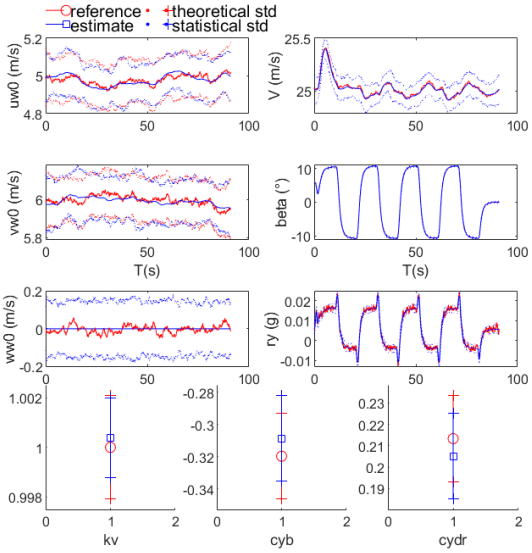

Figure 5: Monte Carlo analysis, MAP lateral calibration model with constraint $w_{w_0} = 0$

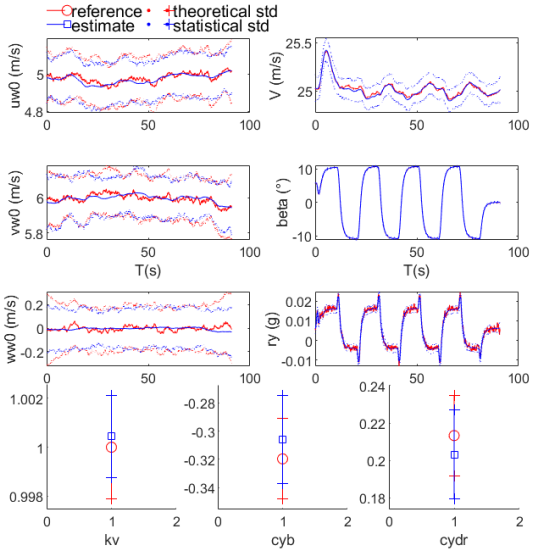

Figure 6: Monte Carlo analysis, MAP lateral calibration model with constraint $\overline{w_{w_0}} = 0$

Table 1 presents, for each estimator, results of a Monte Carlo type analysis carried out on estimated parameters, from a set of fifty simulations generated with different measurement noises and turbulence wind sequences. For the MAP estimator results are also presented in Figures 5 and 6 for constraints $w_{w_0} = 0$ and $\overline{w_{w_0}} = 0$ respectively. In these Figures, reference (or simulation) values are represented in red and estimated values in blue. Solid lines for states or outputs, or squares/circles for parameters, depict the mean values whereas doted lines for states or outputs, or "+" for parameters, depict the confidence interval. These results prove that off-line estimation methods allow to decrease the bias on estimated parameters with respect to parameters estimated by an EKF. Different off-line methods give similar results with slightly smaller bias and measured uncertainties for the MAP estimator. For this latter estimator, constraints $w_{w0} = 0$ or $\overline{w}_{w0} = 0$ produce similar accuracy on estimated parameters. We can notice as well that the MAP estimator is more tolerant to initialisation errors than the other methods.

Table 1: Bias and standard deviation on estimated calibration parameters of the lateral model

	Parameter	EKF	IEKS	FE	MAP	MAP ($\overline{w_{w_0}} = 0$)
Bias	k	-0.0010	0.0003	-0.0015	0.0004	0.0004
	C_{Y_β}	0.095	0.075	0.032	0.014	0.011
	$C_{Y_{\delta_r}}$	-0.071	-0.057	-0.024	-0.010	-0.008
Th. std[a]	k	0.0021	0.0021	0.0021	0.0021	0.0021
	C_{Y_β}	0.016	0.019	0.027	0.027	0.029
	$C_{Y_{\delta_r}}$	0.012	0.014	0.020	0.020	0.022
Stat. std[b]	k	0.0028	0.0020	0.0020	0.0017	0.0016
	C_{Y_β}	0.056	0.068	0.030	0.027	0.031
	$C_{Y_{\delta_r}}$	0.042	0.051	0.023	0.020	0.024

[a] Theoretical standard deviation (Cramer Rao bound)
[b] Statistical standard deviation

Virtual angle of attack sensor and Pitot tube calibration

The general model used for estimation is the one presented in eq. (12). The evolution model for the components of the wind velocity is the model of eq. 5 then we have $f(x(t), \theta, u(t)) = 0$ in (12). Measurements used for estimation are the modulus of the airspeed (V_m) and the vertical acceleration (r_{z_m}) with estimator observation equations respectively given in eq. (7) and eq. (11). The covariance matrix of the measurement noise is $R = \text{diag}([r_1^2,\ r_2^2])$ with $r_1 = 1$ m/s and $r_2 = 0.2$ m/s^2.

DOI: 10.13009/EUCASS2022-7135

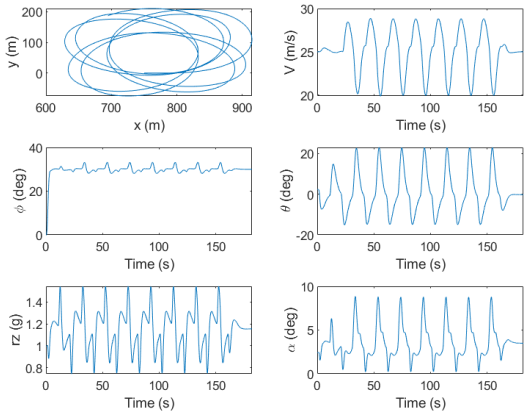

Figure 7: Vertical calibration manoeuvre, oscillations of period 20 s on r_z

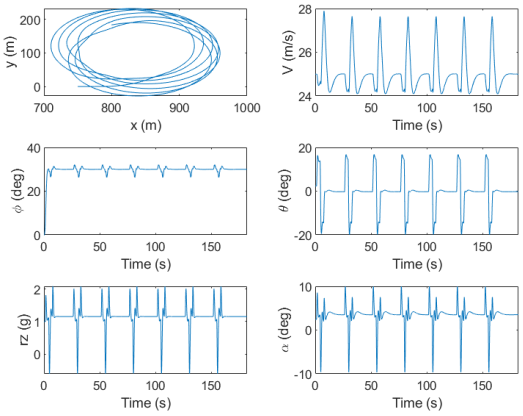

Figure 8: Vertical calibration manoeuvre, oscillations of period 6 s on r_z

As for calibration of the SSA virtual sensor, a specific manoeuvre is defined in order to estimate the AOA virtual sensor parameters ($\tilde{C}_{L_0}$, $\tilde{C}_{L_\alpha}$ and $\tilde{C}_{L_q}$) together with the Pitot tube calibration factor (k). In order to make the overall parameters observable, the manoeuvre must present attitude changes as well as vertical acceleration changes. But besides that, attitude and acceleration changes must act at different frequencies. To illustrate this requirement, two manoeuvres are defined. Both are composed of a 30 degrees roll angle constant turn for attitude changes and vertical acceleration oscillations, of period 20 s for the first manoeuvre (cf. Figure 7) and of period 6.3 s for one oscillation and imposed every 6 s for the second manoeuvre (cf. Figure 8).
A constant mean horizontal wind is also simulated with components $u_{w0} = 5\ m/s$, $v_{w0} = 6\ m/s$ and $w_{w0} = 0\ m/s$.

Observability of parameters from these two manoeuvres is analysed using the output error estimator from a non noisy simulation. Estimator of eq. (22) is applied with $\theta = [u_{w0},\ u_{w0},\ u_{w0},\ k,\ \tilde{C}_{L_0},\ \tilde{C}_{L_\alpha},\ \tilde{C}_{L_q}]^T$. The Cramer Rao bounds on the estimated parameters given by the method for the two manoeuvres are compared in Table 2. We can see that

Table 2: Standard deviation on estimated parameters of the vertical OE model

Parameter	manoeuvre 1	manoeuvre 2	manoeuvre 2 with $w_{w0} = 0$
u_{w0}	0.0024	0.0024	0.0024
v_{w0}	0.0024	0.0024	0.0024
w_{w0}	0.0294	0.0294	
k	0.0006	0.0006	0.0006
$\tilde{C}_{L_0}$	0.0047	0.0051	0.0004
$\tilde{C}_{L_\alpha}$	0.0139	0.0083	0.0081
$\tilde{C}_{L_q}$	0.5400	0.2016	0.2005

for both manoeuvres, uncertainties on w_{w0} and $\tilde{C}_{L_q}$ are important. Uncertainty on $\tilde{C}_{L_q}$ is particularly high for the first manoeuvre. The identified parameters correlation matrix is presented in Figure 9 for the first manoeuvre. It reveals that parameters w_{w0}, $\tilde{C}_{L_0}$,$\tilde{C}_{L_\alpha}$ and $\tilde{C}_{L_q}$ are correlated. For the second manoeuvre, a few correlations disappear (cf. Figure 10), particularly correlation between w_{w0} and $\tilde{C}_{L_q}$ as well as correlation between $\tilde{C}_{L_0}$ and $\tilde{C}_{L_q}$, which explains the improvement on uncertainty on parameter $\tilde{C}_{L_q}$. However, correlation between $\tilde{C}_{L_\alpha}$ and $\tilde{C}_{L_q}$ still remains as well as a strong correlation between w_{w0} and $\tilde{C}_{L_0}$. Then, as for the lateral calibration estimator, it is necessary to impose a constraint on w_{w0} in order to suppress this latter correlation. We then retain manoeuvre 2 for vertical virtual sensor calibration with $w_{w0} = 0$ in vertical estimator model except for the MAP estimator where we can easily impose the mean value of w_{w0} be zeros. Standard deviation of estimated parameters obtained by the OE estimator with $w_{w0} = 0$ are also presented in Table 2. It shows that uncertainty on parameter $\tilde{C}_{L_0}$ is improved in comparison with results without constraint on w_{w0}.

Vertical calibration parameters are now estimated with the different estimators. The EKF estimator model is described

DOI: 10.13009/EUCASS2022-7135

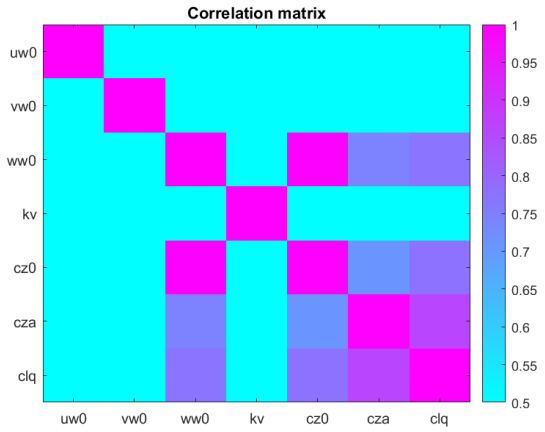

Figure 9: Estimated parameters correlation matrix (OE vertical calibration manoeuvre 1)

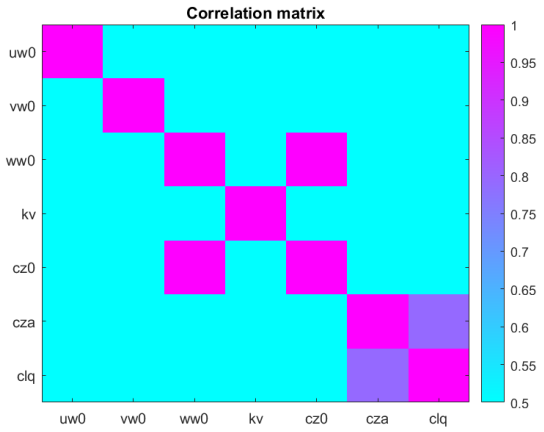

Figure 10: Estimated parameters correlation matrix (OE vertical calibration manoeuvre 2)

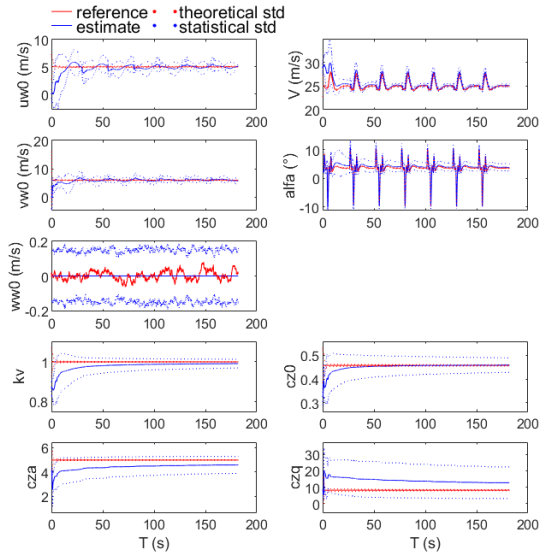

Figure 11: Monte Carlo analysis, EKF vertical calibration model

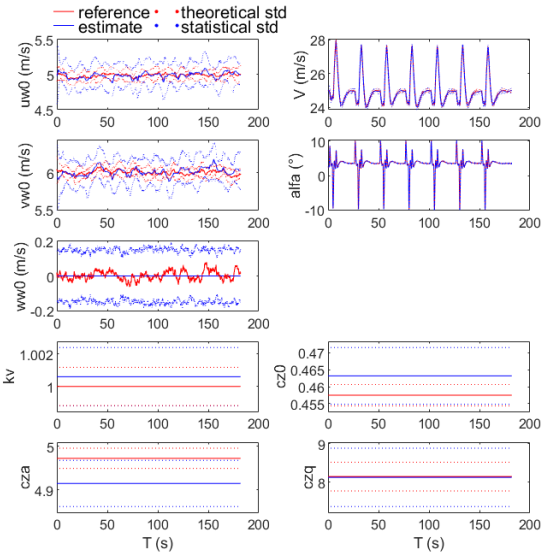

Figure 12: Monte Carlo analysis, IEKS vertical calibration model

in eq. (12) with $x = [u_{w0},\ v_{w0},\ k,\ \tilde{C}_{L_0},\ \tilde{C}_{L_\alpha},\ \tilde{C}_{L_q}]^T$, $Q = \text{diag}([q_1^2,\ q_2^2,\ 0,\ 0,\ 0,\ 0])$ and $P_0 = \text{diag}([p_{0_1},\ p_{0_2},\ p_{0_3},\ p_{0_4},\ p_{0_5},\ p_{0_6}])$. As for the lateral parameters calibration, evolution noise level is tuned such that $q_1 = q_2 = 0.1$ m/s$^{\frac{3}{2}}$ which corresponds to the maximum possible evolution noise preventing estimator divergence. Then simulations are performed with a turbulent wind of level $\sigma_x = \sigma_y = 0.2$ m/s and $\sigma_z = 0.15$ m/s. IEKS algorithm is also applied to the aforementioned model.
The filter error estimator of eq. (20) and the maximum a posteriori estimator of eq. (25) are applied such that $x = [u_{w0},\ v_{w0}]^T$ and $\theta = [k,\ \tilde{C}_{L_0},\ \tilde{C}_{L_\alpha},\ \tilde{C}_{L_q}]^T$.

Figures 11 to 14 present, for each estimator, a Monte Carlo type analysis carried out on estimation results from a set of fifty simulations generated with different measurement noise and turbulence wind sequences. For the parameters, results are also gathered in Table 3. These results prove that off-line estimation methods allow to improve results obtained from an EKF, in a more noticeable manner than for the lateral calibration case. Off-line methods give similar results.

DOI: 10.13009/EUCASS2022-7135

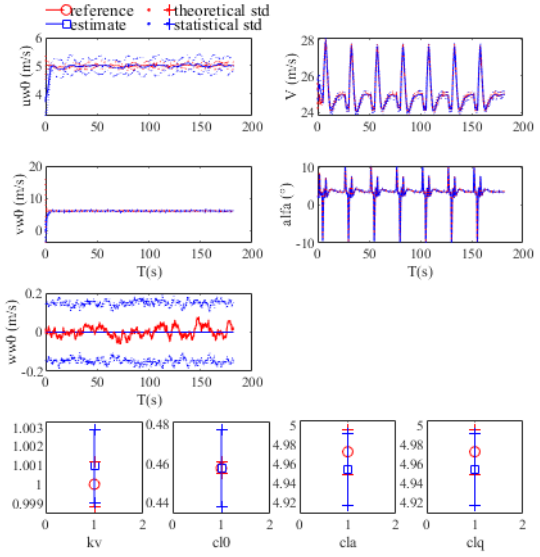

Figure 13: Monte Carlo analysis, FE vertical calibration model

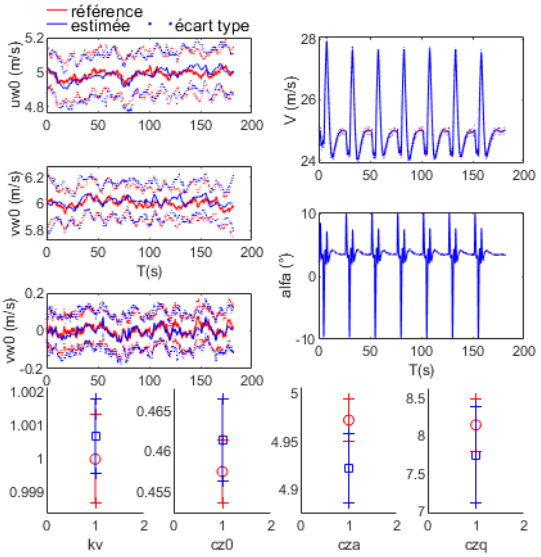

Figure 14: Monte Carlo analysis, MAP vertical calibration model with constraint on mean w_{w_0}

Table 3: Bias and standard deviation on estimated calibration parameters of the vertical model

	Parameter	EKF	IEKS	FE	MAP	MAP ($\overline{w_{w_0}} = 0$)
Bias	k	-0.0087	0.00048	0.00096	0.00094	0.00068
	$\tilde{C}_{L_0}$	0.0014	0.0056	0.00025	0.0043	0.0039
	$\tilde{C}_{L_\alpha}$	-0.4027	0.0614	-0.0187	-0.0439	-0.0508
	$\tilde{C}_{L_q}$	4.5690	-0.0013	-0.6179	-0.2050	-0.3970
Th. std[a]	k	0.0011	0.0014	0.0011	0.0011	0.0013
	$\tilde{C}_{L_0}$	0.0026	0.0033	0.0029	0.0031	0.0039
	$\tilde{C}_{L_\alpha}$	0.0200	0.0231	0.0232	0.0200	0.0227
	$\tilde{C}_{L_q}$	0.3336	0.3741	0.3767	0.3203	0.3510
Stat. std[b]	k	0.0218	0.0019	0.0019	0.0017	0.0011
	$\tilde{C}_{L_0}$	0.0303	0.0073	0.0198	0.0074	0.0051
	$\tilde{C}_{L_\alpha}$	0.6901	0.0585	0.0369	0.0427	0.0362
	$\tilde{C}_{L_q}$	9.6661	0.8216	0.6286	0.6929	0.6445

[a] Theoretical standard deviation (Cramer Rao bound)
[b] Statistical standard deviation

4.2 On-line wind estimation

Once virtual sensors and Pitot tube have been calibrated, calibration parameters are supposed to be known and their values are the estimated values obtained with the MAP estimator. They are gathered in vector ($\hat{\theta}$). Then on-line estimation of the three wind velocity components is realized with an EKF. The estimator model is the one presented in eq. (12). The state vector is $x = [u_{w0},\ v_{w0},\ w_{w0}]^T$ and the wind velocity evolution model is the one of eq. 5, which leads to $f(x(t), \theta, u(t)) = 0$ in (12). Measurements used for estimation are the modulus of the airspeed V_m and the lateral and vertical accelerations (r_{y_m} and r_{z_m}) with estimator observation equations given in eq. (7) and eq. (11). Power spectral density (PSD) of the evolution noise is $Q = \text{diag}([q_1^2,\ q_2^2\ q_3^2])$ and covariance matrix of the measurement noise is $R = \text{diag}([r_1^2,\ r_2^2,\ r_3^2])$ with $r_1 = 1$ m/s and $r_2 = r_3 = 0.2$ m/s^2.
The objective is to be able to estimate wind velocity during operation flight phases and particularly straight and level flight trajectory. Then the scenario chosen to validate our estimator is a straight and level flight subject to a wind gust and turbulence.
The wind gust is modelled as a wind speed amplitude evolution and is function of the distance parallel to the vehicle's flight path. Following EASA and MIL certification specifications concerning gust shape used for limit gust loads

DOI: 10.13009/EUCASS2022-7135

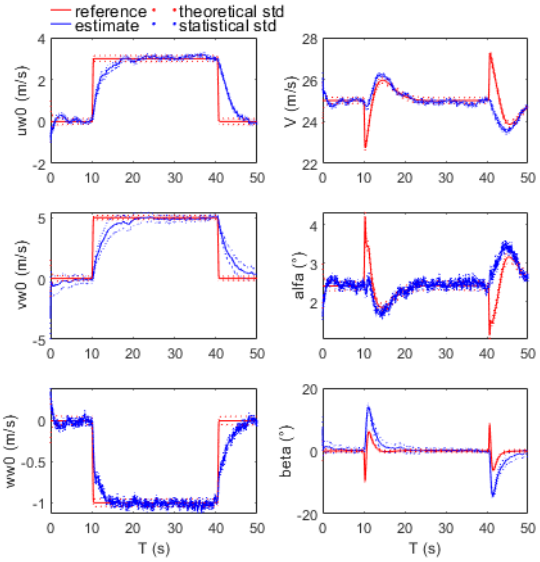

Figure 15: Monte Carlo analysis, on-line wind estimate with EKF - no measurement noise and no turbulence - PSD evolution noise 0.1^2 m^2/s^3

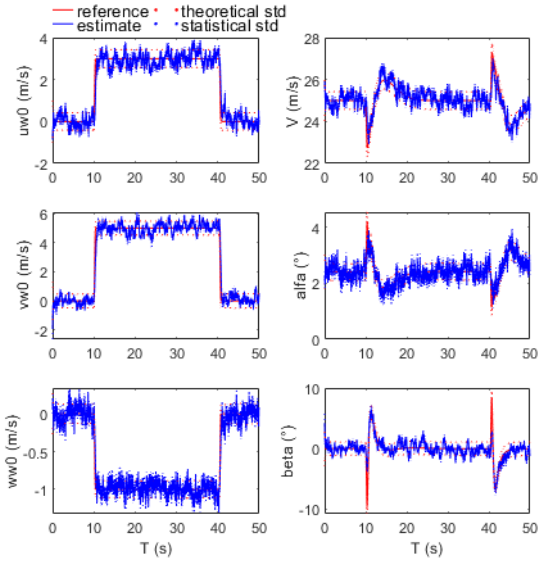

Figure 16: Monte Carlo analysis, on-line wind estimate with EKF - no measurement noise and no turbulence - PSD evolution noise 1 m^2/s^3

computation, the gust shape is composed of an amplitude increase in (1-cos) shape from zero, followed by a constant wind amplitude during 30 s and then a decrease in (1-cos) to zero. The maximum gust amplitude chosen is 5.8 m/s (u_{w0} =3 m/s, v_{w0} =5 m/s, w_{w0} =-1 m/s) and gust gradient (i.e. distance parallel to the vehicle's flight path covered so that the gust reaches its maximum amplitude from 0) is 9 m.

As calibration parameters values are estimated, uncertainties on these parameters as well as correlations between parameters are taken into account in the simulation validation process by adding correlated noises to the parameters values whose covariance matrix is obtained from estimated covariances matrices obtained for lateral and vertical models, multiplied by 9 (3 σ uncertainty bound). Noise on calibration parameters covariance matrix is then:

$$\mathrm{cov}(\hat{\theta}) = 1 \times e^{-3} \begin{bmatrix} 0.0014 & -0.0012 & 0.0008 & 0.0004 & 0.0062 & -0.0634 \\ -0.0012 & 1.0983 & -0.8271 & 0 & 0 & 0 \\ 0.0008 & -0.8271 & 0.6278 & 0 & 0 & 0 \\ 0.0004 & 0 & 0 & 0.0098 & -0.0020 & 0.0165 \\ 0.0062 & 0 & 0 & -0.0020 & 0.4086 & -4.9981 \\ -0.0634 & 0 & 0 & 0.0165 & -4.9981 & 104.1732 \end{bmatrix}$$

Figures 15 and 16 present estimation results for simulations performed without turbulence, with PSD of evolution noise such that $q_1 = q_2 = 0.1$ m/s$^{\frac{3}{2}}$ (tuning chosen for calibration estimators) and $q_1 = q_2 = 1$ m/s$^{\frac{3}{2}}$ respectively. Estimation results, for fifty different noise sequences on parameters and measurement noise, are gathered in a Monte Carlo type analysis. This analysis shows that uncertainty on calibration parameters is negligible in comparison with measurement and evolution noise levels. It also shows that, in both cases, gust is estimated but with delay for the low level evolution noise. An increase of the evolution noise covariance matrix, possible because all state variables are observable with this estimator model, allows a strong limitation of this delay. But as the EKF estimator acts as a low pass filter with a bandwidth proportional to the ratio between evolution noise and measurement noise covariance matrices, an increase of evolution noise level, considering that the measurement noise covariance matrix is fixed, increases the bandwidth. As shown in the figures, a low level tuning results in a smoother estimate than a bigger one. We choose to keep the tuning $q_1 = q_2 = 1$ m/s$^{\frac{3}{2}}$. If simulated turbulence input is considered as evolution noise, then this latter tuning corresponds to moderate intensity turbulence ($\sigma_x = \sigma_y = 2$ m/s and $\sigma_z = 1.5$ m/s).

Results of Monte Carlo type analysis for fifty different runs of noise on parameters, measurement noise and turbulence are plotted in Figures 17 and 18. For both figures, the evolution noise is $q_1 = q_2 = 1$ m/s$^{\frac{3}{2}}$. Results in Figure 17 correspond to a simulation including a gust together with a light turbulence ($\sigma_x = \sigma_y = 0.2$ m/s and $\sigma_z = 0.15$ m/s) whereas results in Figure 18 are obtained simulating turbulence with a moderate level ($\sigma_x = \sigma_y = 2$ m/s and $\sigma_z = 1.5$ m/s) and without gust. These results prove that the estimator is appropriated not only to estimate wind speed evolution during a gust but also to accurately estimate wind speed evolutions due to turbulence of moderate level.

DOI: 10.13009/EUCASS2022-7135

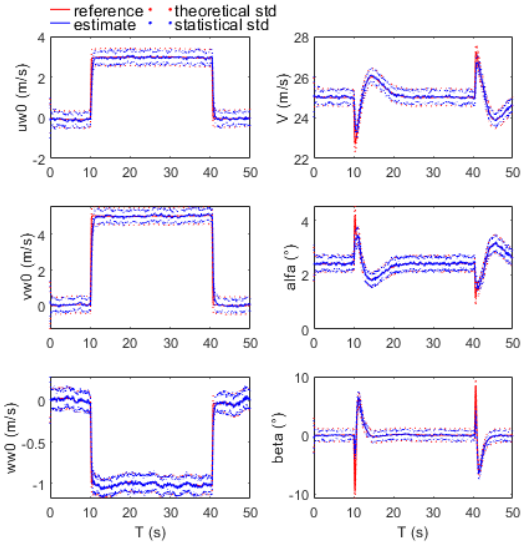

Figure 17: Monte Carlo analysis, on-line wind estimate with EKF - PSD evolution noise 1 m^2/s^3 - simulation with light turbulence

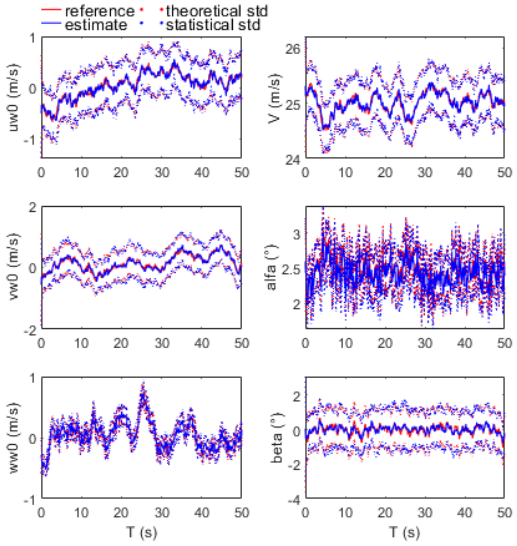

Figure 18: Monte Carlo analysis, on-line wind estimate with EKF - PSD evolution noise 1 m^2/s^3 - simulation with moderate turbulence

On-line wind estimation has been realised fully in the Simulink environment. The estimation algorithm is a discrete time version of the EKF with an analytical linearisation of the observation model around the current state. Different estimation algorithm implementations have been tested and computation times measured from a simulation of 180 s and with data down-sampled to 25 Hz. The first implementation has been done using Simulink "Matlab Function" blocks with a mean computation time of 0.25 s. Implementation through the Simulink block "Extended Kalman Filter" has also been tested and it results in a computation duration multiplied by 2. Finally, implementation through a C++ Sfunction leads to a computation duration divided by 2 compared to the first implementation.

5. Conclusion

An approach for estimating the three components of the wind speed vector using a sensor suite typical of small fixed wings UAVs has been presented. The strategy consists in the development of three estimators. The first and second ones are used to calibrate virtual SSA and AOA sensors and Pitot tube from specific exciting manoeuvres, whereas the third one uses Pitot tube and virtual sensors calibrated by the first estimator to perform on-line wind estimation for all flight phases.

Calibration of SSA and AOA sensors are realised separately from dedicated manoeuvres. We have shown that those manoeuvres must be chosen carefully in order to make states as observable as possible and prevent as much as possible correlations between estimated parameters; they have to be composed of attitude variations as well as acceleration variations (lateral for the SSA virtual sensor calibration and vertical for the AOA virtual sensor calibration) which must act at different frequencies in the case of vertical accelerations. Even with adapted manoeuvres, some correlations remain which we dealt with imposing constraints on the vertical component of the wind speed as well as imposing the initial value of the Pitot tube calibration factor to be rather accurate (error less than 10%). Moreover, we have shown that calibration flights have to be performed in quite atmosphere. Results of different off-line estimation methods (IEKS, FE and MAP) which have been presented are improved compared to those obtained by an EKF. The three tested off-line methods give similar results but the MAP estimator turned out to be more tolerant to errors on initial parameters as well as more efficient in computation time if the number of points chosen for the wind model is not too large. It was shown by Monte Carlo analysis that virtual sensors parameters and Pitot tube calibration factor can be estimated with a good confidence and a low level of bias and uncertainty.

The on-line wind estimation is realised by an EKF based on the virtual sensors and airspeed measurement model calibrated at the previous step. It is shown that the on-line wind speed estimator is able to estimate a sudden wind gust with no delay as well as turbulence of medium intensity. We have also checked by Monte Carlo analysis that uncertainty on calibrated parameters has little impact on wind estimates.

All results presented in this paper have been obtained from simulated data. This approach now has to be assessed on flight test data.

DOI: 10.13009/EUCASS2022-7135

References

[1] G. Balmer, T. Muskardin, S. Wlach, and K. Kondak. Enhancing model-free wind estimation for fixed-wing UAV. In *Proceedings of International Conference on Unmanned Aircraft Systems, ICUAS 2018*, pages 1242–1247, 2018.

[2] M. Brossard, J.-P. Condomines, and S. Bonnabel. Tightly coupled navigation and wind estimation for mini UAVs. In *Proceedings of AIAA Guidance, Navigation, and Control Conference*, Kissimee, United States, January 2018.

[3] W.L. Chan, C.S. Lee, and F.B. Hsiao. Real-time approaches to the estimation of local wind velocity for a fixed-wing unmanned air vehicle. *Measurement Science and Technology*, 22(10), 2011.

[4] A. Cho, J. Kim, S. Lee, and C. Kee. Wind estimation and airspeed calibration using a UAV with a single-antenna GPS receiver and Pitot tube. *IEEE Transactions on Aerospace and Electronic Systems*, 47(1):109–117, 2011.

[5] J.-P. Condomines, M. Bronz, G. Hattenberger, and J.-F. Erdelyi. Experimental wind field estimation and aircraft identification. In *Procedings of the International Micro Air Vehicles Conference and Flight Competition (IMAV 2015)*, Aachen, Germany, sep. 2015.

[6] H. Cox. On the estimation of state variables and parameters for noisy dynamic systems. *IEEE Transactions on Automatic Control*, 9(1):5–12, 1964.

[7] M.A. Efroymson. *Multiple Regression Analysis*, chapter 17 of Mathematical Methods for Digital Computers. John Wiley, New York, 1960.

[8] T. A. Johansen, A. Cristofaro, K. Sorensen, J. M. Hansen, and T. I. Fossen. On estimation of wind velocity, angle-of-attack and sideslip angle of small UAVs using standard sensors. In *2015 International Conference on Unmanned Aircraft Systems (ICUAS)*, pages 510–519, 2015.

[9] V. Klein. Determination of airplane model structure from flight data using splines and stepwise regression. Technical Report 2126, Nasa, March 1983.

[10] V. Klein and E.A. Morelli. *Aircraft System Identification: Theory and Practice*. AIAA, 2006.

[11] J. W. Langelaan, N. Alley, and J. Neidhoefer. Wind field estimation for small unmanned aerial vehicles. *Journal of Guidance, Control, and Dynamics*, 34(4):1016–1030, 2011.

[12] F. A. P. Lie and D. Gebre-Egziabher. Synthetic air data system. *Journal of Aircraft*, 50(4):1234–1249, 2013.

[13] R. E. Maine and K. W. Iliff. Formulation and implementation of a practical algorithm for parameter estimation with process and measurement noise. *SIAM Journal on Applied Mathematics*, 41(3):558–579, 1981.

[14] H. E. Rauch, F. Tung, and C. T. Striebel. Maximum likelihood estimates of linear dynamic systems. *AIAA Journal*, 3(8):1445–1450, 1965.

[15] A. Rautenberg, M.S. Graf, N. Wildmann, A. Platis, and J. Bange. Reviewing wind measurement approaches for fixed-wing unmanned aircraft. *Atmosphere*, 9(11), 2018.

[16] P. Tian, H. Chao, M. Rhudy, J. Gross, and H. Wu. Wind sensing and estimation using small fixed-wing unmanned aerial vehicles: A survey. *Journal of Aerospace Information Systems*, 18(3):132–143, 2021.

[17] A. Wenz, T. Johansen, and A. Cristofaro. Combining model-free and model-based angle of attack estimation for small fixed-wing UAVs using a standard sensor suite. In *2016 International Conference on Unmanned Aircraft Systems (ICUAS)*, Arlington, VA, USA, june 7-10 2016.